IOP Conf. Series: Materials Science and Engineering **966** (2020) 012137 doi:10.1088/1757-899X/966/1/012137

Application of laser interferometry to analyze cutting tool state during machining

I A Efimovich[1] **and I S Zolotukhin**[1, 2]

[1] Institute of Industrial Technology and Engineering, Tyumen Industrial University, 38 Volodarskogo Street, Tyumen, 625000, Russia

E-mail: [2] zolotuhinis@tyuiu.ru

Abstract. The efficiency of a cutting tool can be enhanced through stress–strain and temperature studies. Existing mathematical methods implement simplified boundary conditions, and experimental methods that are either inapplicable to real working conditions or lack the necessary accuracy. This study aims to develop novel experimental methods for stress–strain and temperature field analyses. The approaches entail recording the side deformation fields of the cutting tool by laser interferometry during its operation, separating the deformation fields caused by the cutting forces and heating, as well as calculating the stress–strain and temperature fields using the Young's modulus, Poisson's ratio, and coefficient of linear thermal expansion of the tool material. The advantages of these methods include their applicability under real cutting conditions and the possibility to study the stress–strain and temperature fields of a tool during non-stationary operation by high-speed video recording. The study proves the efficiency of the proposed methods by the orthogonal machining of difficult-to-cut steel disc using a cemented carbide tool with positive rake angle. As a result, the temperature and principal stress fields in the tool were determined. Developed methods can help in the study of cutting tool efficiency.

1. Introduction

The performance of the cutting tool has the greatest impact on the efficiency of the entire machining process, and methods of enhancing this performance are discoverable through the study of the stress–strain and temperature states of the tool in near-real conditions.

Presently, calculation methods that employ analytically obtained boundary conditions with extensive simplifications and assumptions are widely used to determine the stress–strain and temperature states of the tool [1, 2]. To improve the reliability of the calculation results, the experimentally obtained boundary conditions must be used. Many experimental methods have been developed to measure the strain–stress and temperature distributions in the cutting tool.

The use of various types of strain gauges to study deformation fields is extremely challenging because of the extremely small size of the working tool involved, as well as the high temperatures involved in the cutting process. The brittle-coating method is usable for only qualitative analysis, presents significant measurement errors, and is unsuitable for studying dynamic stress–strain fields. The split–tool dynamometer [3] provides an opportunity to determine the stress distributions along only tool faces.

The grid method is partially applicable to high-strength tool materials, considering the difficulty in determining the changes in the node's distances because of the minimal material deformation. Furthermore, the Moire-Fringe method is very time-consuming, owing to the complexity in obtaining

and using gratings. The digital image correlation (DIC) technique is of particular interest; however, it is difficult to be used for studies near the contact zone because of the smallness and inconsiderable tool material deformation.

The photoelastic [4] technique is inappropriate for experiments with real cutting tools and workpiece materials because of the low heat resistance of optically active materials, and it is applicable only at extremely low cutting speeds when processing soft materials. Applying photoelastic coatings partly solves these problems; however, the accuracy is dramatically affected when the coatings peel off in a high strain and temperature gradient zone.

The caustic method [5] differs with the complexity of caustic pattern analyses, especially for a complex stress state with non-uniformly distributed boundary conditions. Electronic speckle pattern interferometry, besides out-of-plane displacements, can be applied to in-plane deformation measurements; however, this method has the same disadvantages as the DIC in the context of cutting tool studies.

The holographic interferometry method is highly sensitive and is applicable to complex-shaped or rough-surface objects. Digital holography partially solves the problem of acquiring and processing holographic interferograms. In laser interferometry, it is necessary to polish the flat surface of the object being investigated; however, interference fringe analysis causes fewer difficulties. All-optical techniques have common problems with their implementation for studying non-static and under vibration objects, such as cutting tools. Moreover, there are difficulties in computing stress components from deformation fields owing to the complicated mathematical processing of the experimental results.

In temperature measurements, the tool-work (natural) thermocouple method is widely used. A variation of this method entails a case wherein the split tool allows measuring the temperature distributions along only the tool faces. However, the split tool properties differ significantly from those of the real metal cutting tool. A method, which employs semi-artificial and embedded artificial thermocouples [6] that are distributed into the body or on the faces of the cutting tool, prevents temperature measurements near the tool edge and differs with the complexity of the tool-making process. The running thermocouple method [7] is unusable in conditions of low feed rates or high cutting speeds and requires complex experiment preparation.

Methods based on the hardness and microstructural changes of a material [4] are utilizable for only the high-speed steel tool because the hardness and structure of the cemented tungsten carbide tool are not significantly affected by temperature changing.

Thermal indicator methods, among which the temperature-sensitive paint method and the physical vapor deposition (PVD) film are notable, are of special interest. However, measuring the temperature fields with a high gradient and a wide range by these methods is quite difficult due to the thermophysical differences between the cutting tool material and the coating. The tempering colors (oxide layer) method cannot be used for quantitative analysis of temperature.

The infrared thermometry method is used most extensively because it provides an opportunity to determine dynamic temperature fields in a non-contact manner. However, due to emissivity dependence on the oxidation state and roughness of the surface, method accuracy highly depends on the accuracy of the selected emissivity coefficient, which can change with surface heating [8].

2. Method

To overcome the limitations of the above-mentioned approaches and improve the process of determining the stress and temperature fields of the cutting tool, we developed methods [9, 10] and experimental rig based on laser interferometry.

These methods are implemented for conditions of orthogonal cutting process. During machining, cutting tool deforms due to the heating and forces acting on it. The shape change and displacement of the tool-side surfaces are determined by changing location of the interference fringes obtained by the interferometer.

The tool state may be depicted by the two-dimensional problem because the cutting tool width is narrow relative to its size, and stresses with temperature may be regarded as uniformly distributed over the tool thickness. Owing to the symmetrical deformation of the tool-side surfaces, a tool width change caused by cutting forces Δt_f and thermal expansion Δt_t at the point of interest may be obtained:

$$\Delta t_f = \frac{\Delta m_f \cdot \lambda}{n} \ , \ \Delta t_t = \frac{\Delta m_t \cdot \lambda}{n} \tag{1}$$

Where Δm_f and Δm_t are the differences in the interference fringe order at the point of interest, caused by cutting forces and thermal expansion, respectively; n is the refractive index of air; and λ is the laser wavelength. The fringe order differences Δm_f and Δm_t may be found by:

$$\Delta m_f = m_1 - m_2 \ , \ \Delta m_t = m_2 - m_0 \tag{2}$$

Where, m_0, m_1, and m_2 represent the fringe order obtained before the process (for cold tool), in the process (for loaded tool), and immediately after cutting was interrupted (for heated tool), respectively.

The strain caused by cutting forces in parallel to the tool edge direction may be found by:

$$\varepsilon_z = \frac{\Delta t_f}{t} = \frac{\Delta m_f \cdot \lambda}{n \cdot t} \tag{3}$$

Where, t is the width of the cold tool measured before cutting. According to Hooke's law,

$$\varepsilon_z = -\frac{\mu}{E} \cdot (\sigma_x + \sigma_y) = -\frac{\mu}{E} \cdot S \tag{4}$$

Where, E is the Young's modulus, μ is the Poisson's ratio, σ_x, σ_y are the normal stresses, and S is the sum of the normal stresses.

Combining (3) and (4), we obtain:

$$S = -\frac{E}{\mu} \cdot \frac{\Delta m_f \cdot \lambda}{n \cdot t} \tag{5}$$

By analyzing the fringe pattern points and using equation (5), we can obtain the distribution of the stress sum S along the closed boundary of the tool. Before stress separation, we must obtain the field of the sum S by finding a solution of the Laplace's equation:

$$\nabla^2 S = 0 \tag{6}$$

To solve the Laplace's equation and realize stress separation, an iterative finite difference method in the Cartesian coordinate system was used. The x-axis of the coordinate system was matched with the clearance tool face (figure 1). C and C_1 in the figure represent the tool-chip and the tool-workpiece contact length, respectively.

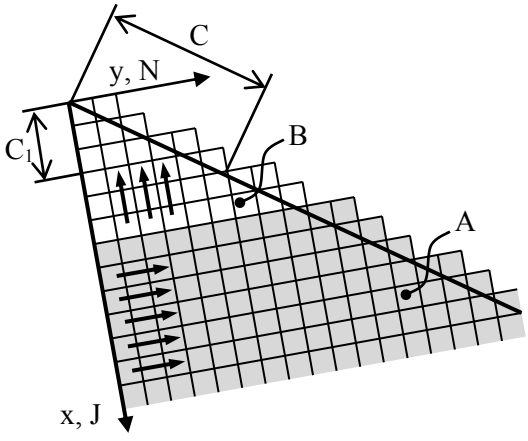

Figure 1. A grid used in the implemented finite difference method.

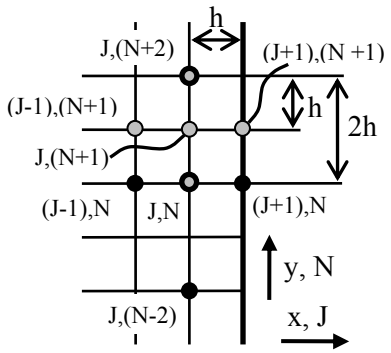

Figure 2. Scheme to calculate stresses at end nodes of grid lines.

Considering the tool state as a two-dimensional stress system and neglecting body forces, the differential equations of equilibrium are as follows:

$$\frac{\partial \sigma_x}{\partial x} + \frac{\partial \tau_{xy}}{\partial y} = 0 \ , \ \frac{\partial \sigma_x}{\partial x} + \frac{\partial \tau_{xy}}{\partial y} = 0 \tag{7}$$

Differentiating equations (7) with respect to x and y gives:

$$\frac{\partial^2 \sigma_x}{\partial x^2} + \frac{\partial^2 \tau_{xy}}{\partial x \partial y} = 0 \ , \ \frac{\partial^2 \sigma_y}{\partial y^2} + \frac{\partial^2 \tau_{xy}}{\partial x \partial y} = 0 \tag{8}$$

Subtracting equations (8) and replacing $\sigma_x = (S - \sigma_y)$, we obtain the main equation for stress separation:

$$\frac{\partial^2 \sigma_y}{\partial x^2} + \frac{\partial^2 \sigma_y}{\partial y^2} = \frac{\partial^2 S}{\partial x^2} \tag{9}$$

In zone A (figure 1), the calculation of σ_y is done in the direction from the boundary, which is out of contact with the chip and workpiece, into the tool body, line by line. In a grid line with $N = 0$, stresses σ_y and τ_{xy} are zero owing to the no-load condition outside the contact boundary. To calculate σ_y in a grid line with $N = 1$, we have to use the following equation:

$$\sigma_{y\,J,1} = \frac{1}{2} \cdot \left(S_{J+1,0} - 2 \cdot S_{J,0} + S_{J-1,0} \right) \tag{10}$$

Equation (10) is derived from a finite difference form of equations (7) and (9), considering the zero value of σ_y и τ_{xy} in the $N = 0$ line.

The stress σ_y in the nodes of lines $N > 2$ may be found by using the finite difference form of equation (9):

$$\sigma_{y\,J+1,N} + \sigma_{y\,J,N+1} + \sigma_{y\,J-1,N} + \sigma_{y\,J,N-1} - 4 \cdot \sigma_{y\,J,N} = S_{J+1,N} - 2 \cdot S_{J,N} + S_{J-1,N} \tag{11}$$

By rearranging it with respect to $\sigma_{y\,J,\,N+1}$, $\sigma_{y\,J+1,\,N}$, $\sigma_{y\,J-1,\,N}$ and $\sigma_{y\,J,\,N-1}$ for extrapolation.

To determine σ_y in the end nodes of the grid lines, first, we have to calculate $\sigma_{y\,J,\,N+2}$ by the following formula:

$$\sigma_{y\,J,N+2} = 4 \cdot \left(S_{J+1,N} - 2 \cdot S_{J,N} + S_{J-1,N} \right) + 10 \cdot \sigma_{y\,J,N} - 4 \cdot \left(\sigma_{y\,J+1,N} + \sigma_{y\,J-1,N} \right) - \sigma_{y\,J,N-2} \tag{12}$$

Equation (12) is derived from equation (11) and transformed with respect to the doubled step $h_y = 2 \cdot h_x$ along the y-axis (figure 2, black nodes). Then, by rearranging equation (11) with centrally used node (J, $N + 1$), we calculate the unknown $\sigma_{y\,J-1,\,N+1}$ and $\sigma_{y\,J+1,\,N+1}$ for the ($N + 1$) grid line (figure 2, gray nodes).

The calculation stress σ_y in zone B (figure 1) is done similarly, considering only the direction change, i.e., instead of J-lines, the N-lines of zone A are used.

The normal stress σ_x may be determined by:

$$\sigma_x = S - \sigma_y \tag{13}$$

Additionally, the shear stress τ_{xy} may be determined by using equations (7). The principal stresses σ_1 and σ_2 may be found by well-known equations, using the previously obtained stress components. To verify the results, we integrated the corresponding stress components in the contact zone to obtain loads on the tool faces and compared them with the cutting forces measured by a dynamometer.

The tool temperature change at the point of interest is given by:

$$\Delta T = \frac{\Delta t_t}{t} \cdot \frac{1}{\alpha} \tag{14}$$

Where, α is the mean coefficient of linear thermal expansion (CTE) for the cutting tool material. Substituting equation (2) into (14) and considering the temperature T_0 of the cold tool (before cutting), the formula for the temperature at the point of interest is as follows:

$$T = T_0 + \frac{m_t \cdot \lambda}{n \cdot t \cdot \alpha} \quad (15)$$

To obtain the temperature field, the fringe pattern along the closed boundary of the tool must be analyzed, and the temperature at points inside the tool may be determined by using Laplace's equation:

$$\nabla^2 T = 0 \quad (16)$$

3. Experimental bench design

The schematic diagram of the experimental setup used to test our proposed methods is shown in figure 3. A horizontal linear polarized laser beam from the source (1) passes through a beam expander (2), a turning mirror (3), a cubic beam splitter (4), and a quarter-wave plate (5). Then, it becomes circularly polarized and strikes an interferometer, which is formed by an optical wedge (6) and a polished side surface (7) of a cutting tool (8). The optical wedge and the tool are rigidly fastened relative to one another by a tool holder (9), which is fixed in a multidimensional dynamometer (10). A light reflected from the surface of the wedge forms the reference beam. The measurement beam is formed by a light transmitted through the wedge and reflected from the tool. After reflection, both beams change their polarization and recombine. The resulting beam passes back through the quarter-wave plate, obtains vertical linear polarization and strikes the beam splitter, where is reflected in the camera lens (11) direction. The interference fringe patterns recorded by the high-speed camera (12) and the dynamometer signal transformed by the analog-to-digital converter (ADC) (13) with an amplifier (14) were saved on a computer (15).

The applied interferometer design increases interference pattern quality: eliminates relative shifts between the optical wedge and the tool induced by vibration during machining due to their rigid fastening by tool holder; eliminates ghosts due to the use of polarizing optics with antireflective coating.

Figure 4 shows the experimental setup mounted on a conventional lathe, which spindle drive was adjustable. On the lathe carriage was placed the base table with a strain gauge dynamometer (1) and two aluminum rails fixed on it. On one rail a laser (2), an achromatic Galilean beam expander (3) (Thorlabs GBE20-A), and a turning mirror (4) were mounted. To achieve a high quality of fringe patterns a single-frequency diode-pumped solid-state laser LCM-S-111 with λ = 532 nm was used.

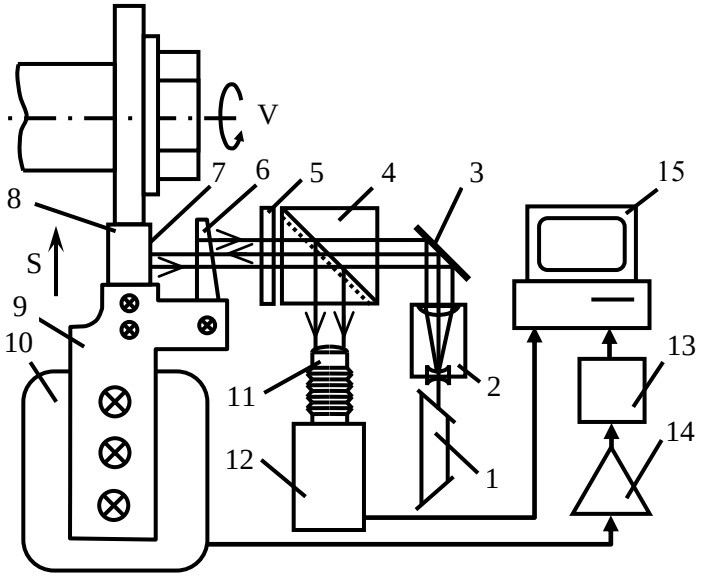

Figure 3. Schematic diagram of experimental setup.

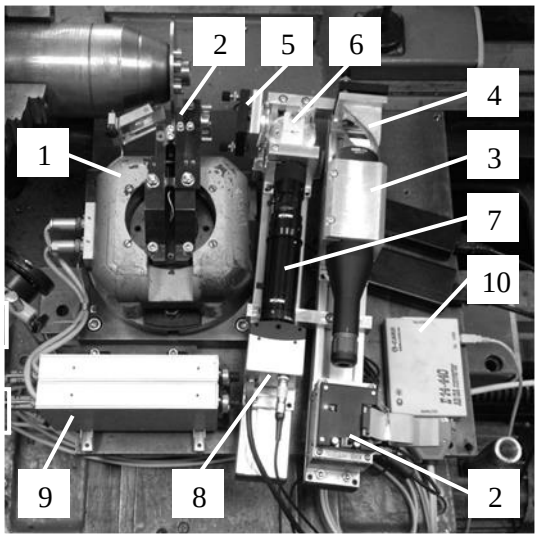

Figure 4. Experimental setup on a lathe.

The second rail carried the rotation mount (5) with a quarter-wave plate, tilt-rotation stage (Standa 6PT110) with a cubic beam splitter (6), and a zoom camera lens (7) (NAVITAR Zoom 6000) attached to a high-speed digital camera (8) (Fastec HiSpec 2). A strain gauge amplifier (9) (RDP621) connected to the ADC (10) (L-Card E14-440) was placed on the base, near the dynamometer.

4. Experimental details

To prove the efficiency of the proposed methods, a machining experiment on a disc of 4.2-mm thickness was performed. Martensitic heat-treated steel grade X13Cr11Ni2W2MoV with hardness HB 275 was used as a work material. Table 1 presents its chemical composition. This steel is difficult-to-cut and widely used for the production of turbine parts, like blades and discs.

Table 1. Chemical composition of heat-treated steel X13Cr11Ni2W2MoV.

Element	C	Cr	Ni	W	Mo	V	Si	Mn	S	P	Fe
wt.%	0.10–0.16	10.5–12.0	1.5–1.8	1.6–2.0	0.35–0.50	0.18–0.30	max 0.6	max 0.6	max 0.025	max 0.03	bal.

The tool material was cemented tungsten carbide WC-8Co grade VK8. The cutter had a 4.65 mm width, 25° rake and 10° clearance angles. The machining conditions were: cutting speed V of 6 m/min and feed rate S of 0.14 mm/rev. The camera frame rate was 16×10^3 fps.

5. Results and Discussion

Figure 5 presents the interference patterns recorded by camera (a) before at $T_0 = 20$ ºC, (b) in the process of cutting, and (c) immediately after cutting interruption.

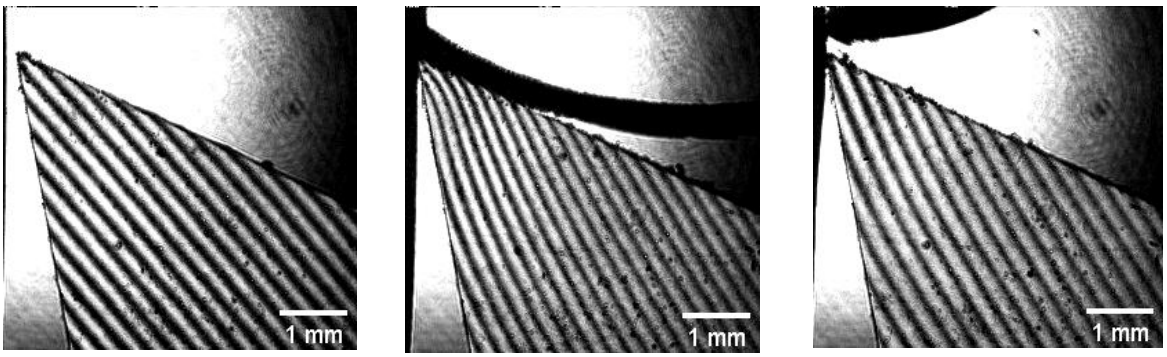

a b c

Figure 5. Images of interference fringes recorded (a) before, (b) in the process, and (c) immediately after cutting interruption.

The fringe order distribution curves were obtained by analysis of image profiles along the closed boundary in ImageJ. As a boundary, lines along the rake face, the clearance face, and the line forming triangle with them were used. Figure 6 shows the curves of fringe order for the (a) rake and (b) clearance faces, which represent the index number of each profile maxima and their location l on the face respect to the tool edge. Plotting and curves subtracting were done by built-in MS Excel functions.

The fringe order m were converted to sum of the stresses S and temperature change ΔT by using the CTE [11], Young's modulus and Poisson's ratio of the cemented tungsten carbide WC-8Co. Figures 7 and 8 show the principal stresses σ_1, σ_2, and the temperature fields, respectively, which were computed by a specially created program in MATLAB to realize the aforementioned methods.

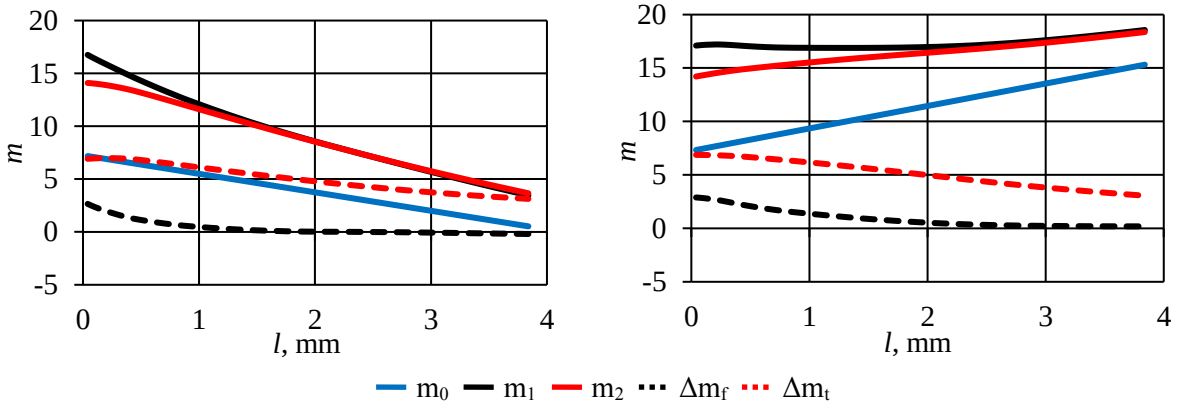

a b

Figure 6. Curves of fringe order *m* for the (a) rake and (b) clearance faces.

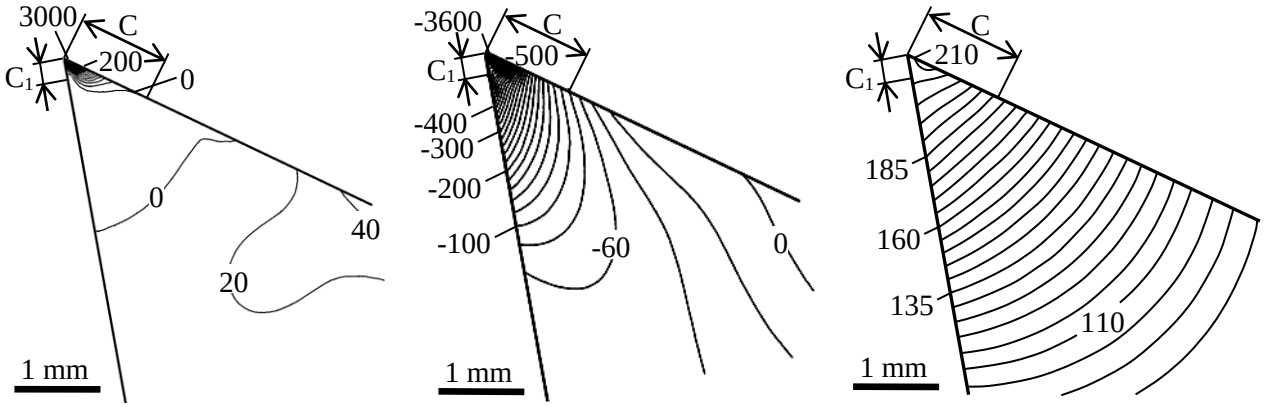

a b

Figure 7. Fields of principal stresses (a) σ_1 and (b) σ_2 (in MPa)

Figure 8. Temperature field (in Celsius degree).

6. Conclusion

The developed experimental methods are applicable under real cutting conditions and may be used for the thermal and stress-strain analyses of a tool composed of real cutting material, including non-stationary conditions during its operation because of the use of a high-speed digital camera.

References

[1] Arrazola P J, Özel T, Umbrello D, Davies M and Jawahir I S 2013 *CIRP Ann.-Manuf. Techn.* **62** 695-718
[2] Shi B and Attia H 2010 *Mach. Sci. Technol.* **14** 149-88
[3] Buryta D, Sowerby R and Yellowley I 1994 *Int. J. Mach. Tool. Manu.* **34** 721-39
[4] Trent E M and Paul K W 2000 *Metal cutting* 4th ed. (Boston: Butterworth-Heinemann) p 464
[5] Isogimi K, Kitagawa T and Kurita H 1988 *Int. J. Jpn. S. Prec. Eng.* **54** 390-5
[6] Komanduri R and Hou Z B 2001 *Tribol. Int*. **34** 653–82
[7] Astakhov V P 1998 *Metal Cutting Mechanics* (Boca Raton: CRC Press) p 320
[8] Pujana J, del Campo L, Pérez-Sáez R B, Tello M J, Gallego I and Arrazola P J 2007 *Meas. Sci. Technol.* **18** 3409
[9] Efimovich I A, Zolotukhin I S and Shvetsova E I 2010 *RF Patent Specification* no. 2442967
[10] Efimovich I A and Shvetsova E I 2009 *RF Patent Specification* 2436039
[11] Efimovich I A, Zolotukhin I S and Zav'yalov E S 2019 *Obrabotka Metallov. Metal Working and Material Science* **21** 129–40